Modelling the Kinetics of Pyrolysis Oil Hydrothermal Upgrading Based on the Connectivity of Oxygen Atoms, Quantified by ^{31}P-NMR

Mahdi Sharifzadeh [a,1], Christian J. Richard [b,c], Nilay Shah [a]

[a] Centre for Process Systems Engineering (CPSE), Department of Chemical Engineering, Imperial College London, South Kensington, London SW7 2AZ, UK.
[b] Department of Chemical Engineering, Imperial College London, South Kensington, London SW7 2AZ, UK.
[c] Mass Spectrometry Facility, Kings College London, Franklin Wilkins Building, London SE1 9NH.

Abstract- In the light of current environmental concerns, pyrolysis of biomass offers a carbon neutral pathway to cheap renewable fuels known collectively as pyrolysis oil (PO). However, crude PO is not immediately usable in the current energy infrastructure and needs to be deoxygenated via upgrading technologies. Upgrading reactions are invariably complex since the chemical components in PO can run into hundreds. Moreover, these components are often very difficult to characterize, posing difficulties towards tracking their chemical reactivity and the overall kinetics as a function of time. To address this problem, the aim of this work is to present a modelling strategy to help researchers predict the kinetics of PO deoxygenation in hot compressed water, under hydrothermal conditions, near to or at the supercritical region. To do this, a trial reaction network superstructure with the maximum degrees of freedom was formulated and evaluated for the deoxygenation of three different Oils. This superstructure was based on the connectivity of an oxygen atom matrix which was quantified based on hydroxy groups by quantitative ^{31}P{H} NMR. The complexity of the large-scale superstructure was subsequently simplified by trimming insignificant arcs; subject to an empirical understanding of the underlying chemistry. By parameter estimations, reaction networks were validated or rejected, depending on whether the computationally simulated data for a given reaction network fits the experimental results. It is anticipated that the development of the disclosed "proof of concept" models could promote the chemical understanding and hence optimisation of hydrothermal upgrading technologies.

---

[1] **Corresponding Author:** Dr Mahdi Sharifzadeh; Room C603, Roderic Hill Building, South Kensington Campus, Imperial College London, UK. SW7 2AZ. E-mail: mahdi@imperial.ac.uk; Tel: +44(0)7517853422

1. Introduction

The quest to develop environmentally carbon-neutral economies has led to research along many avenues, one of which is the development of pyrolysis oil (PO). POs are the products of biomass pyrolysis and are potentially self-sustainable alternatives to traditional fossil fuels [1–8]. However, raw POs cannot be used in internal combustions engines or blended with fossil fuels since they contain significant amounts of water (ca 30%) and organic oxygenates (40 - 55% of the dry organic oxygen in content PO) [9] which give POs a low calorific value. Moreover PO also contains organic acids which makes it highly corrosive and difficult to store [2,10]. As consequence PO has to be deoxygenated using upgrading methodologies so that it can augment current energy infrastructures. The most widely used means to upgrade PO is hydrodeoxygenation (HDO) [1,11,12]. However, a major drawback to this process is the expensive hydrogen feed and the high water content of PO which is inimical to the hydrodeoxygenation catalysts used [13,14]. An alternative way to deoxygenate PO is to use hydrothermal upgrading (HTU). The origin of this technology was due to Berl in the 1920's, who proposed that hot compressed water (HCW) could be used to upgrade plant-derived biomass; an idea that later led to the Hydrothermal Upgrading (HTU) process by Shell [15,16]. The term "hydrothermal" usually refers to HCW below or up to the critical point of water. The properties of HCW are density dependent and vary according to autogenic, or externally applied pressures [17]. This is especially true near the critical point of HCW (Tc = 373.94°C, Pc = 22.04 MPa, ρ_c = 0.37 g/cm^3) at which HCW dissolves PO to give single phase deoxygenation system [17,18].

It is widely recognized that yield and distribution of hydrocarbon products during biomass pyrolysis and upgrading, strongly depends on the processing conditions [5]. Intensive research is devoted on the kinetic studies of fast pyrolysis of biomass. The common feature of these studies is that the overall kinetic is formulated as superposition of the decomposition of lignocellulosic biomass main ingredients, namely cellulose, hemicellulose and lignin, [19–21]. However, such approach is not immediately scalable to upgrading technologies, as unlike biomass, POs compose of hundreds of species. Model compound analysis has been exploited by several researchers in order to underpin the mechanism and kinetics of hydrothermal upgrading. Besse et el [22] studied catalytic hydrothermal processing of linoleic acid in a mixture containing ethanol/water. They identified a series reaction network, in the order of linoleic acid to stearic acid, then to ethyl stearate, and finally to heptadecane. Peterson, et al [23] studied hydrothermal conversion of glucose-glycine mixtures, which were found highly interactive. Overend and

59 coworkers [24,25] proposed two phenomenological approaches for modelling the kinetics of

60 lignocellulosics fractionation by steam-aqueous pretreatments. Their first approach was based on the

61 assumption that the overall "lumped" system kinetics can be represented by summation of underlying

62 homogenous subsystems. The second approach assumed a continuous distribution for the activation

63 energies. Zhang, et al [26] investigated hydrothermal liquefaction of Enteromorpha prolifera for bio-

64 crude production, using thermogravimetric analysis. Their proposed a two-step mechanism consisted

65 of volatilization reactions followed by thermal reactions. A model including a second-order reaction and

66 a 1-D diffusion model for the first step and a first-order reaction for the second step gave the best fit to

67 the experiment data, in terms of the overall biomass conversion. However, such model does not have

68 any implications for the identity of products or their chemical characteristics. Vo, et al [27], formulated

69 the hydrothermal liquefaction of Aurantiochytrium sp. KRS101 (a microalgal) as the superposition od

70 the decomposition of carbohydrates, lipids, and proteins. Their model can predict the amount of

71 aqueous-phase, bio-oil, and gas products. However, it does not have any implication for the product

72 species or their thermophysical properties. Hietala, et al [28] and Valdez et al [29] developed a kinetic

73 model for hydrothermal liquefaction of microalgeas. Their reaction network established pathways

74 between the solids, bio-crude, aqueous products, and gaseous products. Luo, et al [30] conducted

75 similar research on hydrothermal processing of soy concentrate. Yin, et al [31] investigated

76 hydrothermal decomposition of sewage sludge. Their reaction model includes intermediates such

77 protein, saccharide, NH4 and acetic acid. While, a thorough review of the kinetics studies in the field of

78 hydrothermal upgrading is beyond the scope of the present research, several important conclusions

79 can be drawn from aforementioned analysis:

80 1. Hydrothermal upgrading reactions are highly interactive and exhibit nonlinear behaviours,

81 2. Diverse and numerous components available in the POs, hinder development of kinetic models

82   based on actual species. Often lumped modelling based on the product phase, or conversion of

83   the initial biomass is applied to characterise the extent of the upgrading reactions.

84 3. Existing kinetic models do not provide any insight into the physical and chemical properties of the

85   products, neither they characterize the type of the deoxygenation reactions under hydrothermal

86   conditions.

87 The present research aims at breaking through the abovementioned frontiers by proposing a new kinetic

88 modelling framework based on the connectivity of oxygen atoms. In view of the chemically complex
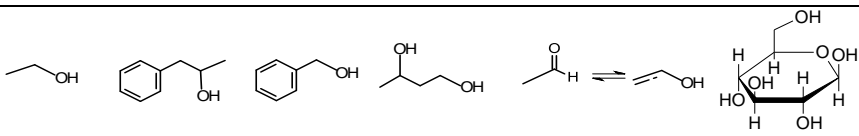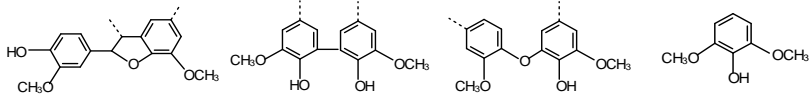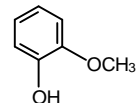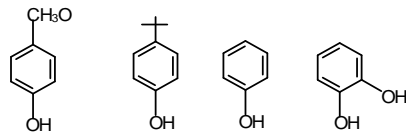
89 nature of PO and its upgraded matrices, the concentration and distribution of all organic oxygenated

90 compounds were classified in terms of hydroxy, (OH), groups. In this way, it was possible to use

91 "lumped" kinetics to simplify the kinetics modelling of PO deoxygenation processes, many of which lead

92 to the removal of OH to form water or gaseous carbon oxides. The use of the OH group was deemed

93 to be satisfactory marker since it both forms a substantial fraction of the overall organic content present

94 in PO and also because of its wide distribution amongst different organic oxygenates [32]. Nonetheless,

95 the dynamics of deoxygenation reactions strongly depend on the strength of the hydroxy groups

96 bounded to organic compounds, and such formulation offers an intuitive way for its characterization.

97 To determine the OH content of the POs they were initially derivatised (phosphytilated) with TMDP

98 according to the following reaction (R-1) [33] so that the entire content of organically bound OH could

99 be conveniently quantified using quantitative $^{31}P\{H\}$ NMR.

(R1)

100
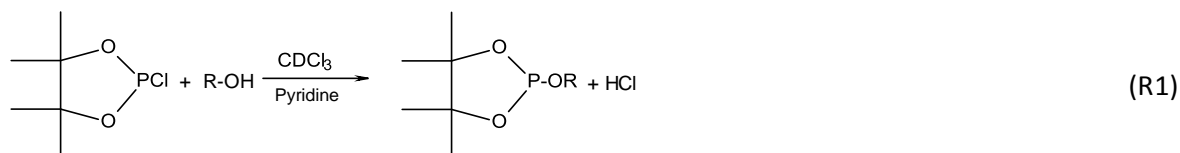
101 This analytical protocol has been widely used [33–39] and gives reproducible results to within a 95%

102 confidence limit [40]. It is also convenient as PO samples can be derivatised directly. However, as

103 TMDP also reacts with water, it is necessary to ensure that the samples are substantially dry. It should

104 be noted that both proton and ^{13}C NMR can be also used to characterise PO. In the case of the ^{1}H

105 nucleus, it is intrinsically 15 times more NMR sensitive than the ^{31}P nucleus despite the fact that the ^{31}P

106 nucleus is 100% naturally abundant. On the other hand, ^{13}C is 100 times less abundant than ^{1}H which

107 means that sensitivity issues become problematic at low analyte concentrations. Notwithstanding, the

108 *dioxaphospholane* adduct shown in reaction (R-1) is very sensitive to the nature of the parent molecule

109 R. This implies that its $^{31}P\{H\}$ NMR chemical shifts are well resolved which means they can easily be

110 used to define the OH groups boundaries shown in Table 1, as validated by extensive OH-containing

111 model compound studies [35]. In Table 1 there are five different groups, each labelled according to the

112 nature of the parent molecules, R, to which the phosphytilated OH groups are bonded.

113

114 **Table 1.** Classification of derivatised hydroxy Groups based on ^{31}P{H} NMR chemical shifts

^{31}P{H} NMR shifts/ ppm	Representative compounds within given groups
OH Group *1*	*Aliphatic OH*
145.4- 150.0 ppm	
OH Group *2*	*C5-Substituted / Syringyl / Condensed Phenolic OH*
137.6 -144.0 ppm	
OH Group *3*	*Guaiacyl OH*
140.0-144.5 ppm	
OH Group *4*	*Phenolic (ρ-Phenolic / Catecholic) OH*
139.0-140.2 ppm	
OH Group *5*	*Carboxylic OH*
133.6-136.0 ppm	
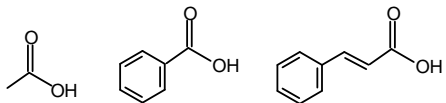
115

116 In Table 1, the Aliphatic Group 1, contains the chemical shifts derived from phosphytilated OH groups

117 not directly bonded to aromatic rings. Aliphatic OH groups are generally the most reactive ones in HCW.

118 For example, glucose contains highly reactive OH groups [41] which come from the cellulose content

119 in plant biomass; this is easily depolymerised in HCW [42]. The Phenolic OH groups in Groups 2, 3 and

120 4 are generally less reactive and are often located on aromatic moieties derived from lignin. It should

121 be noted that lignin is formed from guaiacyl, syringyl, or phenolic phenyl propane precursors shown in

122 Figure 1. These molecules also illustrate how single molecules can contain more than one type of OH

123 Group, classified in Table 1. Group (5) gives representative examples of Carboxylic OH groups on acids

124 such as acetic acid and formic acid. These acids are very important products in the upgraded PO [18].

125 It should be noted that PO oxygenates can range from small to very large molecular weights and contain

126 different types of OH Group. Moreover, the elements in the different OH Groups in Table 1 contain only

127 representative examples of the many hundreds possible compounds.
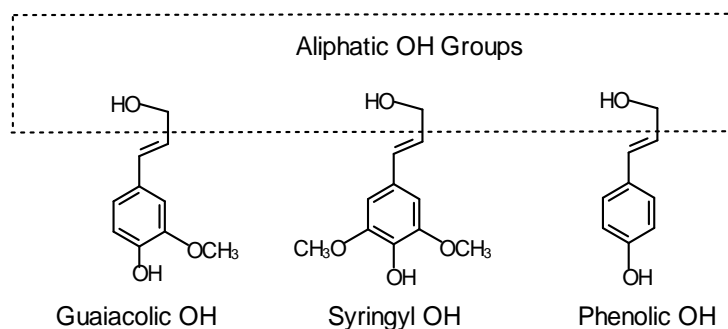
Fig. 1. Aliphatic, Guaiacolic, Syringyl and Phenolic OH groups [43]

The main advantage of the $^{31}P\{H\}$-NMR analytical technique is that the chemical shift boundaries in Table 1, make it easy to classify OH Groups into a form which is suitable for lumped kinetic studies. A main disadvantage is that organically bounded "silent" oxygens which lack a labile hydrogen cannot be derivatised by TMDP. Therefore, they are not detectible using $^{31}P\{H\}$-NMR. This means that the OH containing elements in the five OH Groups in Table 1 are mutually exclusive but not collectively exhaustive. In this work, the "silent" content was calculated by subtracting the oxygen content in the hydroxy groups, quantified by $^{31}P\{H\}$ NMR, from the overall oxygen content obtained from a CHN elemental analysis. The water content was determined using the Karl Fisher technique. The absence of water in the dry processed oil was verified by the virtual absence of a signal at 132.ppm in its 31PNMR spectrum [44].

The formation and destruction of "silent" oxygens are very important during hydrothermal upgrading. For example, Katritzky *et al* studied the reactions of many model compounds in HCW and of these, the reactions of benzyl alcohol **1** are shown in Figure 2, [45,46], which is converted to the ester and ether functionalities in compounds **2**, **3** and **4**.

144
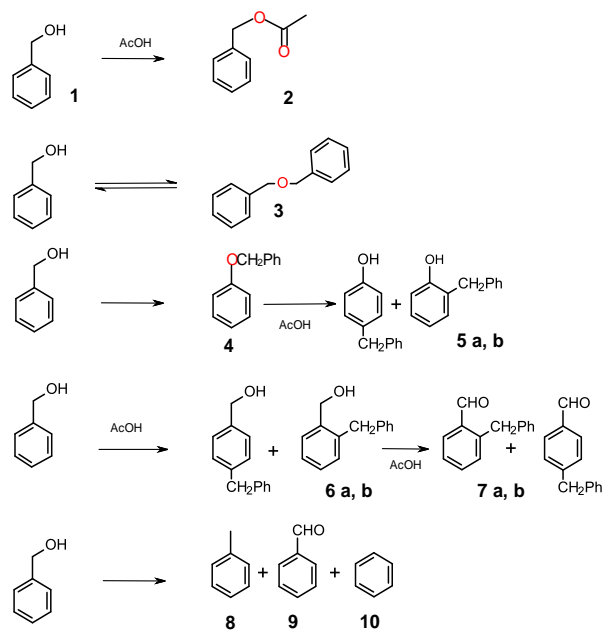
Fig. 2 The cascade reactions of benzyl alcohol in HCW and the formation of "silent" oxygen [45,46].

The oxygen molecules in these compounds are highlighted in red since they are $^{31}P\{H\}$ NMR "silent".

However the aldehyde functionalities (e.g., in compounds **7**(a, b) and **9)**, do react with TMDP [47].

Figure 2 also depicts the loss of aliphatic OH from benzyl alcohol to give the C-C bonds in **4**(a, b) and

7(a, b) and the fully deoxygenated hydrocarbons, **8** (toluene) and **10** (benzene). The hydrogen required

for the total deoxygenation is presumably evolved from the water gas shift reaction [48]. The benzyl

ether, **3**, in Figure 2 is also an example of the importance of OH groups as intermediates in the reversible

formation of silent oxygen species.

A number of models for the hydrothermal pre-treatment of biomass have been published [25,49,50].

However to the best of our knowledge, the reactivity of OH in HCW has not been previously used to

model the deoxygenation kinetics of PO. Since OH groups can be reversibly formed from "silent"

oxygens, it was not possible to produce computationally viable reaction kinetics without a consideration

of the silent oxygens which, taken as a whole, were lumped into a single class in these preliminary

studies. Therefore, each of the model networks used in this work account for the reactive "silent"

oxygenated species in PO, which also undergo reversible reactions between given OH groups. In the

first study of this kind, this paper outlines some kinetic insights into the deoxygenation of upgrading

POs achieved by tracking the concentrations of the listed OH Groups in Table 1 as a function of time;

and by using $^{31}P\{H\}$ NMR to characterise the OH species studied. For the sake of brevity, the details of

experimental results and the numerical values of the optimized model and are presented in the on-line

Supplementary Material (SM).

This section presented the research background and defined the scope of present publication. In the next section, the experimental procedure applied for generating kinetic data is elaborated. Then, the experimental results are presented and key observations are highlighted. Section 4 outlines the modelling framework and proposed two extreme reaction networks with minimum and maximum connectivity between OH groups and products. Section 5 summarizes the mechanic insights gained from the underlying chemistry. The Result Section 6 begins with illustrating the limitations of the two extreme networks. In view of these shortcomings, a tailor-made network is proposed which incorporates the mechanistic insights and its performance is discussed. The paper concludes with summarizing the results and proposing future research directions.

2. Experimental procedure

The POs used in this study, A, B and C, were derived from the fast pyrolysis of Norwegian Spruce, *Picea Abies*, which is an example of a renewable soft woody biomass. A set of five stainless steel tubular batch reactors were constructed and used (volume: 8 cm^3; 12mm outer diameter) for all experiments; these were sealed with compression fittings (Swagelok®). It should be noted that stainless steel has no demonstrated catalytic effect [41,48]. The empty batch reactors were weighed initially, charged with deionised water (3g) and pyrolysis oil (1g) and then purged with argon to remove air. After sealing, the reactors were weighed a second time. POs A and B were then heated in an air recirculating oven to a reaction temperature of 380°C. The reaction times were: $t_0 = 0$, $t_1 = 5$; $t_2 = 6$; $t_3 = 15$; $t_{10} = 10$ minutes. It required 5 minutes to reach the reaction temperature of 380°C in the oven used (Figures S1 in SM). Two extra reaction times were used for the third PO, C: $t_0 = 0$, $t_1 = 5$; $t_2 = 10$; $t_3 = 15$; $t_4 = 20$ and $t_5 = 30$ minutes. After heating, the batch reactors were immediately quenched in ice and left to stand for several hours. The loaded reactors were then externally dried and then reweighed a third time to confirm no potential mass loss had occurred due to leakage. All the liquid products from the hydrothermal upgrading were extracted in acetone, which was then removed by rotary evaporation. Gases were not measured in this preliminary work. It was not possible to measure the autogenic pressures from the home made batch reactors used. A partial solution to this problem was to run the reactions at the reduced density ρ_r (where $\rho_{r = } \rho_{w/} \rho_{w,c}$; ρ_w mass of water(g)/reactor volume) and $\rho_{w,c} = 0.375$ g cm^{-3}) of 1.0 at which the reaction contents would have been expected to form a single phase under reaction conditions specified above [18,51].

194   The POs and their upgraded derivatised products were carried out according to published procedures,

195   with the phosphitylating agent TMDP (2-chloro-4,4,5,5-tetramethyl-1,3,2-dioxapholane). The oil

196   samples were then analysed by quantitative $^{31}P\{H\}$-NMR and the integrated signals were quantified

197   relative to an added standard of known concentration. This protocol is further elaborated in the SM.

198   Each quantitative measurement was the average of duplicate runs. The Oils, A, B and C differed with

199   respect to the processing technology used to prepare them, which was not disclosed by the supplier at

200   Future Blends Ltd. However, all of the oils were freshly prepared and immediately refrigerated to reduce

201   any "aging" reactions.

202   The CHN analysis was done at the University of Sheffield Microanalysis service using a Perkin Elmer

203   2400 CHNS/O Series II Elemental Analyser. The CHN analysis of each sample was the average of

204   three determinations. The oxygen content was determined by mass balance. The results were accurate

205   to within +/- 0.3% of the total mass of the samples.

206   The organic oxygen content was determined in the "raw" pyrolysis oil by mathematically subtracting the

207   water from the CHN analysis. In the dry processed oils, the absence of water was verified by the virtual

208   absence of a signal at 132 ppm in its $^{31}P\{H\}$ NMR spectrum. The use of $^{31}P\{H\}$ NMR to determine small

209   amounts of water was previously reported and also re-investigated [44,52].

210   **3. Experimental results**

211   Three different pyrolysis oils called A, B and C were studied and the initial concentrations of the

212   Aliphatic, Condensed phenolic, Guaiacyl, Phenolic and Carboxylic OH groups were determined by

213     $^{31}P\{H\}$ NMR. The results are shown in Figure 3 which also highlights the five OH Group categories

214   shown, classified in Table 1.
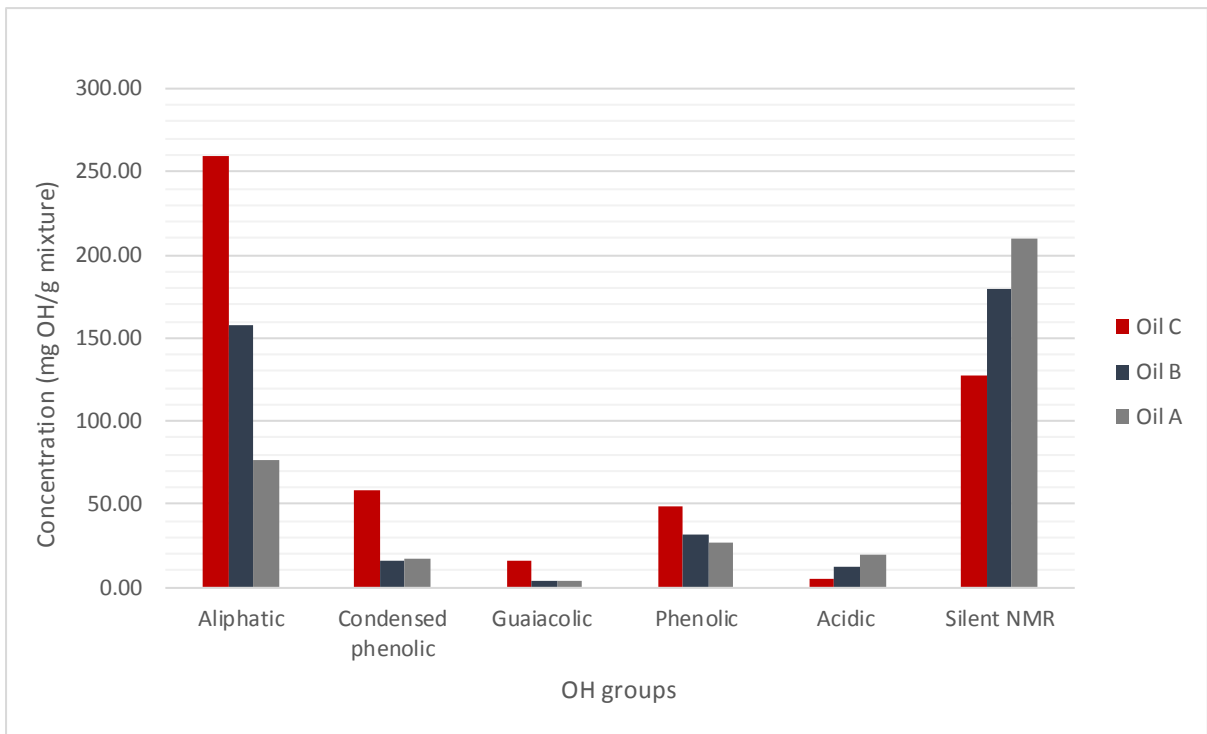
Fig. 3. The concentration of unprocessed Aliphatic, Condensed Phenolic, Guaiacyl, Phenolic, and Carboxylic OH groups in Pyrolysis oils A, B, and C.

Note that Figure 3 does not include the OH groups in water which was removed from the samples. The Norwegian Spruce used to produce these oils has a high proportion of Cellulose [18] which explains the high percentage of Aliphatic OH groups in the oils; but especially of Oil A. The lignin content of Norwegian Spruce also accounts for the Phenolic OH groups in the oils. No attempt was made to characterise any of the chemical species, R that the OH groups were bonded to. However, it is expected that the size, nature and concentration of the R groups would depend on the pyrolysis conditions used to make Oils A, B and C.

In addition of the characterisation of the unprocessed oils, Figure 4 shows the overall concentration of OH and silent O in the upgraded Pyrolysis Oils A, B and C, as a function of time.
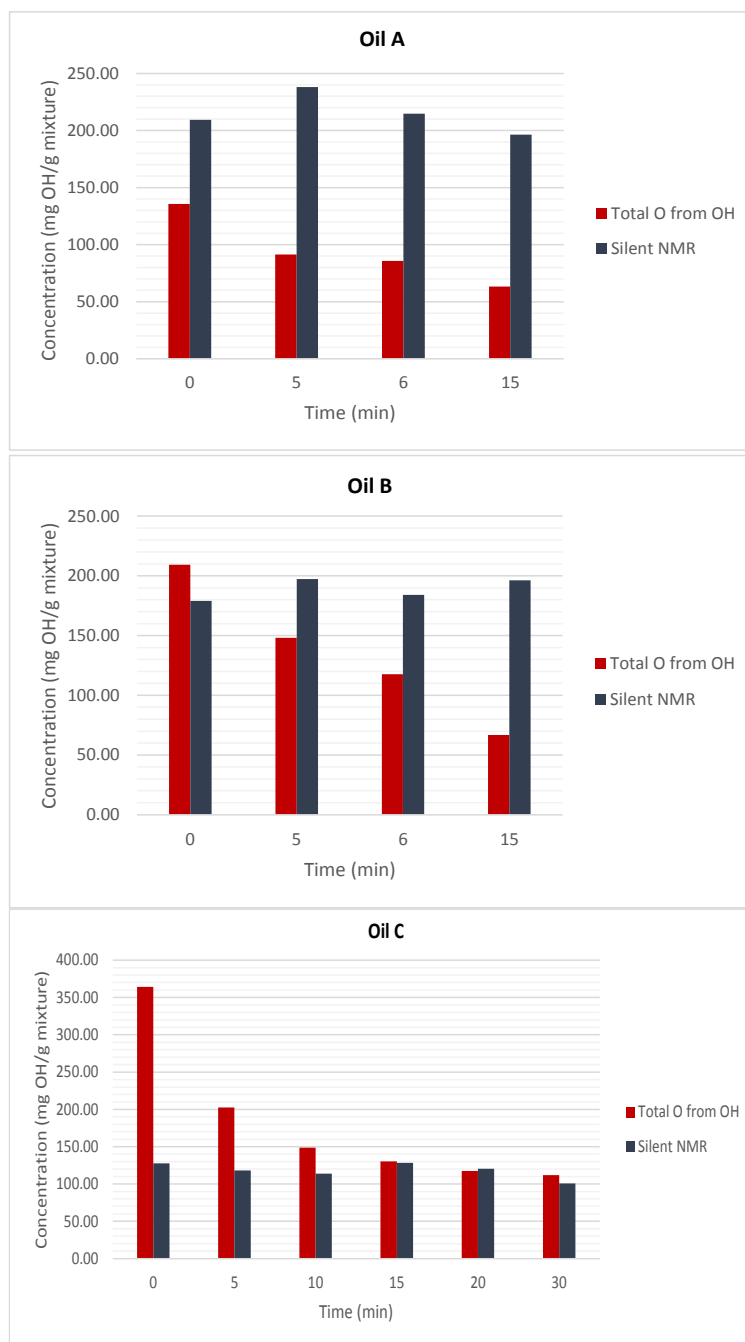
Fig. 4. The overall concentration of OH and O during hydrothermal upgrading reactions for Pyrolysis Oils A, B and C.

For Oils A, B and C, the experimental results are tabulated in Table 2 and categorised according to the

OH group classifications.

Table 2. The experimental results in terms of the concentration of OH groups and NMR-"silent" Oxygen atoms

Time	OH content in P NMR groups					CHN Analysis	
	Aliphatic OH	Condensed Phenolic OH	Guiacyl OH	Phenolic (ρ-Phenolic/ Catecholic) OH	Carboxylic OH	Total O from OH	^{31}P-NMR Silent O
min	mg OH/g mixture	mg OH/g mixture	mg OH/g mixture	mg OH/g mixture	mg OH/g mixture	mg O/g mixture	mg O/g mixture
Oil A							
0	76.15	17.29	4.20	26.75	19.87	135.78	209.46
5	42.90 ↓	8.91 ↓	10.17 ↑	20.66 ↓	14.39 ↓	91.33 ↓	238.14 ↑
6	34.84 ↓	9.48 ↑	10.08 ↓	22.92 ↑	13.83 ↓	85.80 ↓	214.80 ↓
15	23.23 ↓	4.67 ↓	10.14 ↑	17.82 ↓	11.33 ↓	63.24 ↓	196.30 ↓
Oil B							
0	157.69	16.25	4.31	31.86	12.31	209.34	179.02
5	57.27 ↓	27.61 ↑	17.87 ↑	39.03 ↑	15.71 ↑	148.23 ↓	197.38 ↑
6	50.99 ↓	20.00 ↓	12.52 ↓	27.58 ↓	13.87 ↓	117.61 ↓	184.18 ↓
15	24.87 ↓	3.99 ↓	10.50 ↓	19.76 ↓	11.92 ↓	66.86 ↓	196.34 ↑
Oil C							
0	259.04	58.57	16.11	48.51	4.69	364.16	127.79
5	83.60 ↓	38.47 ↓	19.60 ↑	52.40 ↑	21.24 ↑	202.64 ↓	118.15 ↓
10	40.16 ↓	28.55 ↓	21.30 ↑	52.88 ↑	15.27 ↓	148.85 ↓	113.95 ↓
15	30.09 ↓	24.86 ↓	19.49 ↓	51.18 ↓	12.75 ↓	130.22 ↓	128.23 ↑
20	20.91 ↓	22.83 ↓	19.96 ↑	48.64 ↓	12.60 ↓	117.60 ↓	120.39 ↓
30	18.69 ↓	24.86 ↑	18.03 ↓	49.32 ↑	7.81 ↓	111.73 ↓	100.76 ↓

From Figure 4, it is clearly seen that the concentrations of OH and silent O are different for oils A, B and C, presumably due to differences in the compositional makeup of the original oils. However, for modelling purposes it was instructive to tabulate the concentration changes of each type of OH Group according the lumped categories defined in Table 1. This data is presented in Table 2 in which the red arrows and blue are associated with increases and decreases in the OH concentrations, respectively. This table clearly indicate the nonlinear behaviour of the interacting reaction pathways.

From Table 2, it is clear that the consumption of Aliphatic OH groups in oils A, B and C is always dominant and masks any reactions that might have led to the formation of Aliphatic OH groups. However, the increases in Condensed Phenolic OH in Oils A, B and C is presumably related to differences in the nature of the condensed phenolic in each oil. Interestingly, decreases or increases in the concentrations of condensed phenolic OH groups is generally correlated with increases or decreases in the corresponding concentrations of Guaiacyl OH groups. This could be due to reversible reactions of the type depicted by reaction (R-5) in Section 5.8 below. The hydrolysis of the Guaiacyl OH groups would also account for the increased concentration of the Phenolic OH groups according to

250   Reaction (R-6). However, the concentration changes of the condensed phenolic, guaiacyl and phenolic

251   OH groups are not totally correlated in Table 2 which reflects the participation of other undefined

252   reactions. On the other hand, the oxidation of Aliphatic OH groups would account for the increases in

253   the Carboxylic OH groups. Table 2 also gives the initial silent oxygen content of the raw Oils A, B and

254   C as 209.46, 179.02 and 127 mg/g, respectively. This is the hidden oxygen content in functionalities

255   such as ethers, esters, and ketones which cannot be derivatised by TMDP. Differences in the

256   concentrations of these "silent" oxygens in the upgraded oils A, B and C over time, reflects the net

257   balance between the production and destruction of various hydroxy groups. This would not include

258   unreactive silent oxygens some of which would have been present initially in the raw POs. In this

259   respect, it should be noted that the presence of large amounts of a soluble amorphous precipitate,

260   which was found in the upgraded products had a high ^{31}P{H}-NMR "silent" oxygen content, (as

261   determined by a CHN analysis) possibly due to the abundance of aromatic ether linkages which can be

262   difficult to break under hydrothermal conditions [53]. The data in Table 2 was used to produce tentative

263   reaction networks which were formulated by correlating the concentration increases and decreases of

264   each type of OH Group defined in Table 1.

4. Kinetic models and reaction networks

4.1. The formulation of trial reaction networks and their parameter estimation

267   The basic modelling strategy was to produce trial reaction networks in terms of the OH Groups

268   classifications in Table 1. The arcs in each network represented the solutions to a set of ordinary

269   differential equations pertinent to the conversion of given OH Groups listed in Table 1. Following the

270   estimation of the necessary parameters for each network, computer simulations were run and the

271   results evaluated to see if they converged with the experimentally observed OH concentration trends in

272   Table 2.

273   The trial reaction networks presented in Figures. 5, 6, and 11 below were solved using MATLAB. The

274   rate expression was based on Equation 1a and used in the production of each arc in the reaction

275   networks:

276    $\quad -r_A = dC_A/dt = k\, C_A^n$ $\hfill (1a)$

277    $\quad k = k_o \exp\left(-\dfrac{E}{RT}\right), \qquad 0 < n < 2$ $\hfill (1b)$

278   The parameters of these equations were optimized compared to the experimental data trends in Table

279   2. In principle any software tool that can solve ordinary differential equations (ODEs) and minimize the

280   model mismatch for parameter estimation, including for example MATLAB, Aspen Custom Modeller or

281   gPROMS, which could all be used for the present research. In the present research, the MATLAB

282   Genetic Algorithm (GA) was used in conjunction with the FMINCON solver (hybrid GA) so that all the

283   necessary parameters could be estimated. The MATLAB software tool was chosen for the modelling

284   work on account of its built-in Genetic Algorithm toolbox which is a global optimization algorithm for

285   equations which define highly nonlinear systems. The genetic algorithm (GA) uses operators which

286   mimic the evolution of genetic systems. Using a global stochastic search method on a population of

287   potential solutions, GA produces a new set of population points by iterations until the best point in a

288   population approaches an optimal solution [54]. The fitness of the parameters was evaluated in terms

289   of mean square error (MSE):

290 $$Fitness = \sqrt[2]{\sum_{Oil} \sum_{Groups} \sum_{Time} \frac{1}{n} \times (\frac{C_{model\ prediction} - C_{experimental}}{C_{experimental}})^2} \qquad (2)$$

291   In Equations 1a and b, n is the number of experimental data points. The concentrations of OH groups

292   were normalized in order to give a similar weight to the various OH groups. The formulated program

293   had 108 optimization variables (parameters to be estimated) which typically converge to optimized

294   values within a day. In view of the constraints of time, only 4 data points where used for POs A and B.

295   Six points were used in PO, C, for the purposes of comparison.

296 **4.2. Networks with the minimum and maximum degrees of freedom**

297   The first network models to be considered are shown in Figures 5 and 6 in which the OH connectivity

298   are at a minimum and maximum, respectively. In Figures 5 and 6, the lumped Aliphatic (1), Condensed

299   Phenolic (2), Guaiacyl (3), Phenolic (4), and Carboxylic (5) OH Groups are presented as nodes which

300   are depicted as grey circles. In addition to the OH groups, the NMR "silent" oxygens are placed in an

301   additional node. Moreover, Figures 5 and 6 show that the OH groups are ultimately and irreversibly lost

302   to give hydrocarbons, water or gases such as H_2, CO, CO_2 and CH_4; which are also lumped into a final

303   node which called "products" in tables S1-S3 in the SM. The reactions in which PO lost oxygen to form

304   gaseous carbon oxides and water, or in which oxygen was gained from HCW to form PO oxygenates

305   (e.g. the hydrolysis of an ether to form two OH Groups, reaction R-2), were not explicitly defined in this

306   study. Methane also reacts with HCW to give methanol which would also add to the Aliphatic OH content

307   [55]. However, in a previous work we have shown that the gases produced under our reaction conditions

308   are not significant [1].

309　In terms of the OH node connectivity, the trial reaction network in Figure 5 contains the minimum

310　degrees of freedom since it does not account for any creation of different OH groups which are often

311　referred to as "interconversions" in the text.
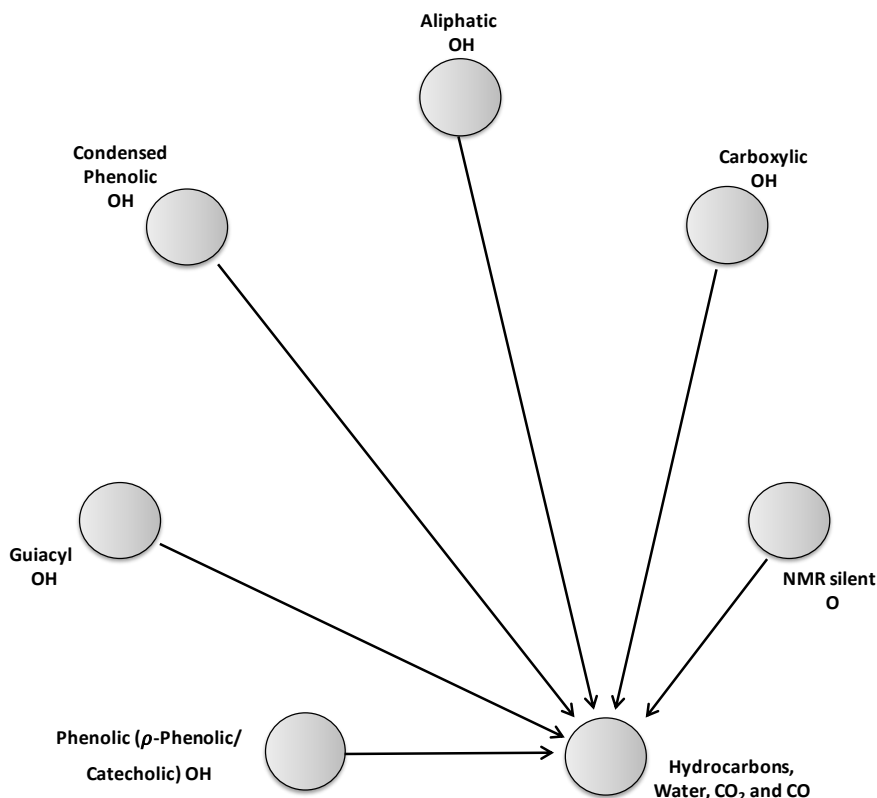
313　**Fig. 5**. The trial reaction Network 1 with the minimum degree of freedom

314　In contrast to Figure 5, the trial network in Figure 6 is formulated in terms of a superstructure reaction

315　network. This has the maximum degrees of freedom. In this way, the destruction of OH groups in one

316　node, or the creation of OH groups in another node, can be mathematically formulated as the

317　interconversion of an OH element from one of the defined Groups to another shown in Table 1.

318　Representative examples of such interconversions are highlighted in the listed equations below

319　(Section 5), many of which are equilibrium reactions. The reaction of OH groups to give "silent" oxygens

320　can also be viewed as the destruction of OH groups. Unfortunately, a main drawback to the network in

321　Figure 6 is that it is computationally expensive. Another drawback is that the least significant arcs are

322　likely to be over emphasized if the experimental data is over fitted. In this case, the convergence of the

323　computationally simulated data with the experimental data would lead to invalid conclusions.

324
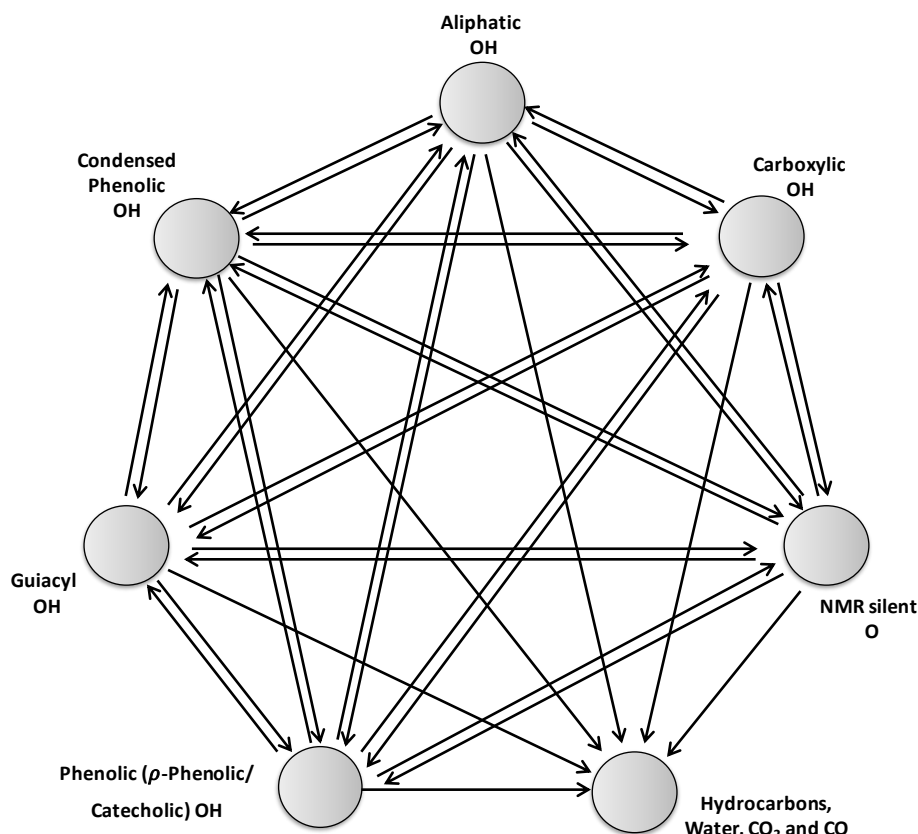
Fig. 6. The reaction Network 2 with the maximum degree of freedom

5. Mechanistic insights into creation and destruction of OH groups

The following sections provide representative examples of chemical reactions which are used to

account for the interconversion of OH Groups.

5.1. Aliphatic OH node → P-NMR Silent O node

This can be exemplified by the dehydration reactions in Figure 2 in which benzyl alcohol loses water to

give esters and ethers (compounds **2** and **3**, and **4**).

5.2. Aliphatic OH node → Carboxylic OH node

Aliphatic alcohols can be oxidized to Carboxylic acids such as formic and acetic acid. In this case, the

original OH group would be lost and a Carboxylic OH is created, together with a "silent" ketonic oxygen.

5.3. Aliphatic OH node → Hydrocarbon Node

Dehydration reactions or reductions with adventitious H_2 remove Aliphatic OH groups to give water.
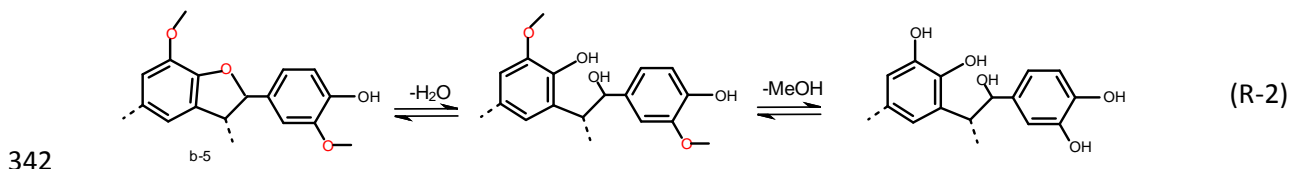
Examples of OH removal are seen in the formation of the carbon bonded phenolic compounds, **6**(a, b)

and **7**(a, b) and products **8** and **10** in Figure 2.

5.4. Condensed Phenolic OH node → Aliphatic OH node

Aliphatic OH groups could be created by the hydrolysis of internal ether linkages as shown by the condensed b-5 phenolic in reaction (R-2).

(R-2)

5.5. Aliphatic OH node→ Condensed Phenolic OH node

Reaction (R-3) is analogous to the reaction which produces the condensed products **6** (a, b) and **7**(a, b) in Figure 2.

(R-3)
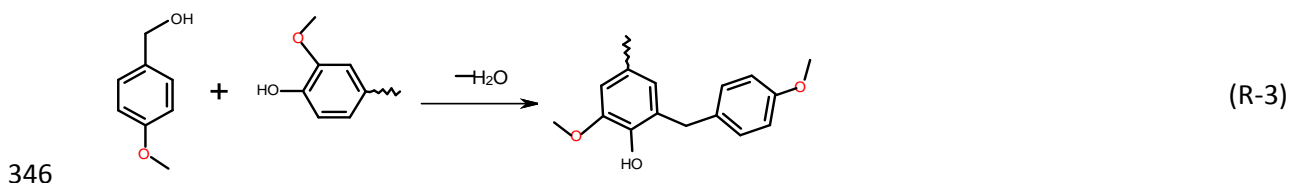
The molecules in reactions (R-2) and (R-3) are derived from lignin, and their corresponding reactions would be expected to occur in HCW.

5.6. Carboxylic OH node → Silent Oxygen node.

The Carboxylic OH groups can be converted into "silent" Oxygen groups by esterification. The formation of the formate ester from formic acid is given in reaction (R-4) and shows how the Carboxylic OH group can be converted into a "silent" Oxygen.

(R-4)

5.7. Carboxylic OH node → Hydrocarbon Node

The Carboxylic node is also linked to the Hydrocarbon Node since carboxylic acids can lose CO_2 to give hydrocarbons, irreversibly. Formic acid could be converted to CO_2 and H_2 [56].

5.8. Guaiacolic OH node → Condensed phenolic OH node

The condensation of the monomers in reaction (R-5) would readily give a condensed phenolic structure in HCW.

(R-5)

5.9 Condensed phenolic OH node → Guaiacyl OH node

The hydrolysis of aryl ethers has been shown to occur in HCW [46] and could provide Guaiacyl OH groups by the reverse of reaction (R-5).

5.10. Guaiacyl OH node→ Phenolic OH node

The hydrolysis of methoxy, (CH_3O), functionalities would create a Phenolic OH group and a methanolic aliphatic OH group which is shown in reaction (R-6) [51].

(R-6)

5.11. Condensed Phenolic OH node → Guaiacyl OH node

In Table 2, decreases in the concentration of condensed phenolic group were associated with rises in the concentrations of Guaiacyl OH concentrations. This would occur by the cleavage of an internal ether, according to the reverse of reaction (R-5).

5.12. Phenolic OH node→ Guaiacyl OH node

This reaction would occur from the reverse of reaction (R-6).

5.13. Phenolic OH node→ Condensed Phenolic OH node

The reaction could occur, for example, by the reversal of reaction (R-5).

5.14. Phenolic OH node→ "Silent" Oxygen node

Phenolic OH groups could be esterified according to reaction (R-4) to give "silent" oxygens. Phenolic OH groups could also become involved in ethers linkages to give Condensed compounds according to reaction (R-5).

6. Results and Discussions

Regarding all of the trial reaction networks studied in this work, Table 3 gives the results of the MATLAB parameter estimations in terms of the value of the objective function used to evaluate the performance of each network in the problem domains. For each network, the average percentage deviations between the experimental data and simulated data is given in Table 3. For the sake of brevity, the full numerical results are reported in the SM. From Table 3, it can be seen that that Networks 1 and 2 have the worst and best performances, respectively with respect to the deoxygenation kinetics of Oils A, B and C. The results are discussed in the following sections in more details.

Table 3. The performance of Reaction Network 1, 2, and 3 in terms of the deviation of the overall model simulations of the experimental results.

	Network #1	Network #2	Network #3
Description	Minimum connectivity	Maximum Connectivity	Empirically Tailored
Fitness (Equation 2)	0.0824	0.0168	0.0288
Average error %	28.71%	12.96%	16.96%

6.1. The parameter estimation results for Network 1 with minimum connectivity

The plotted data in Figure 7 shows that the simulated and experimentally observed changes in OH concentrations do not converge. Therefore, it is evident that the model Network 1 fails to simulate most of the experimental trends in Table 2. However, Figure 7(a-c) shows that Network 1 successfully predicted the observed experimental values for the Aliphatic OH concentrations.
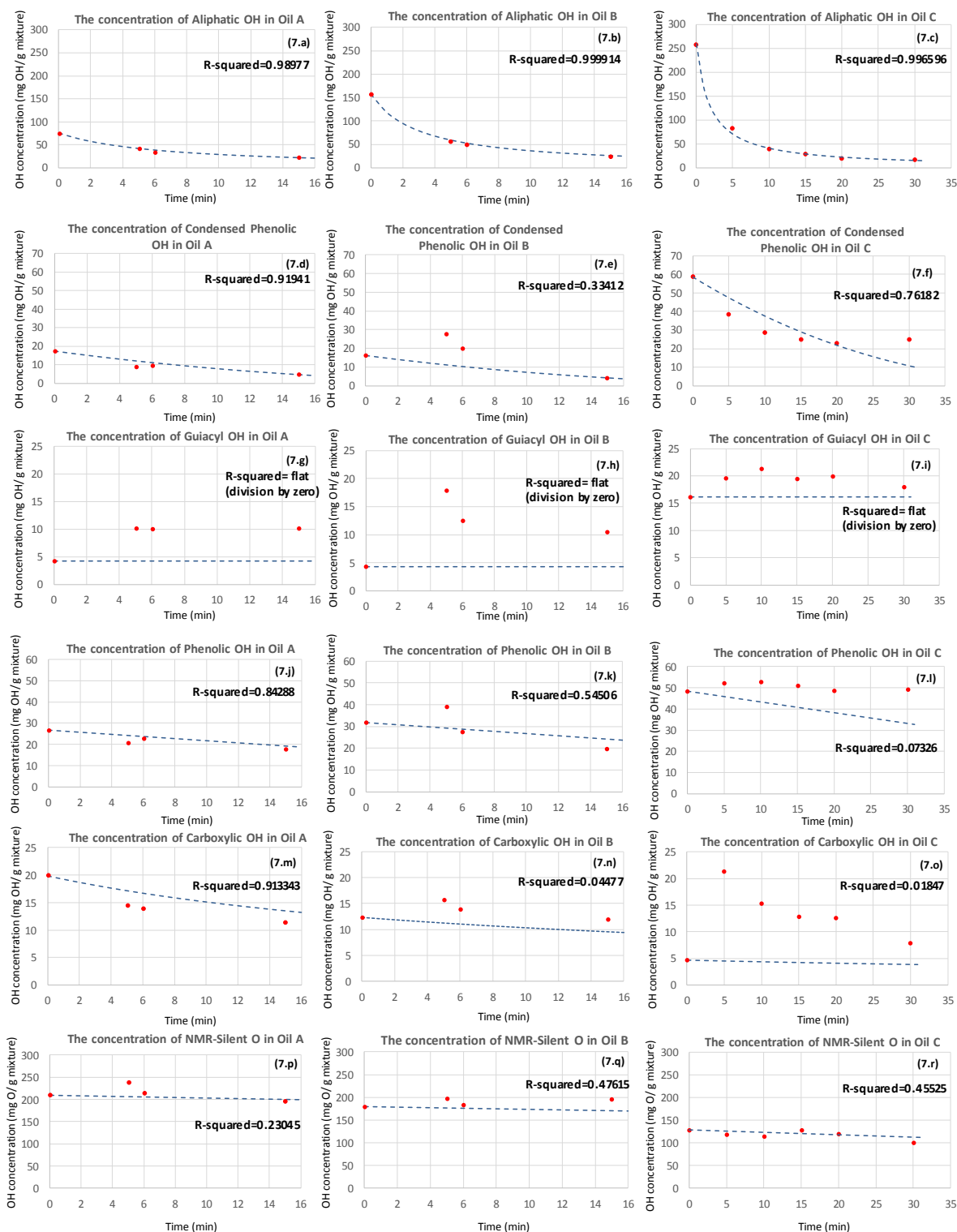
Fig. 7 The performance for model Network 1 with minimum connectivity

Figure 7(g-i) also shows that the simulated values of the Guaiacyl OH group conversions do not

matches the experimentally observed results. The results of parameter estimations suggest flat

concentration for the Guaiacyl group. This is shown by zero pre-exponential factor in Table S1 and by

the grey arc in Figure 8 which shows that the direct conversion of the elements in the Guaiacyl OH

402   Group to hydrocarbons, gases and water was improbable. However, the data trends in Table 2 imply

403   that Guaiacyl OH groups are also being simultaneously created and converted to "silent" species or

404   interconverted to another aromatic OH group. Differences with respect to the creation or removal of

405   Guaiacyl OH groups in Oils B and C are attributed to differences in the initial makeup of Oils B and C

406   as shown in Figure 3.

407
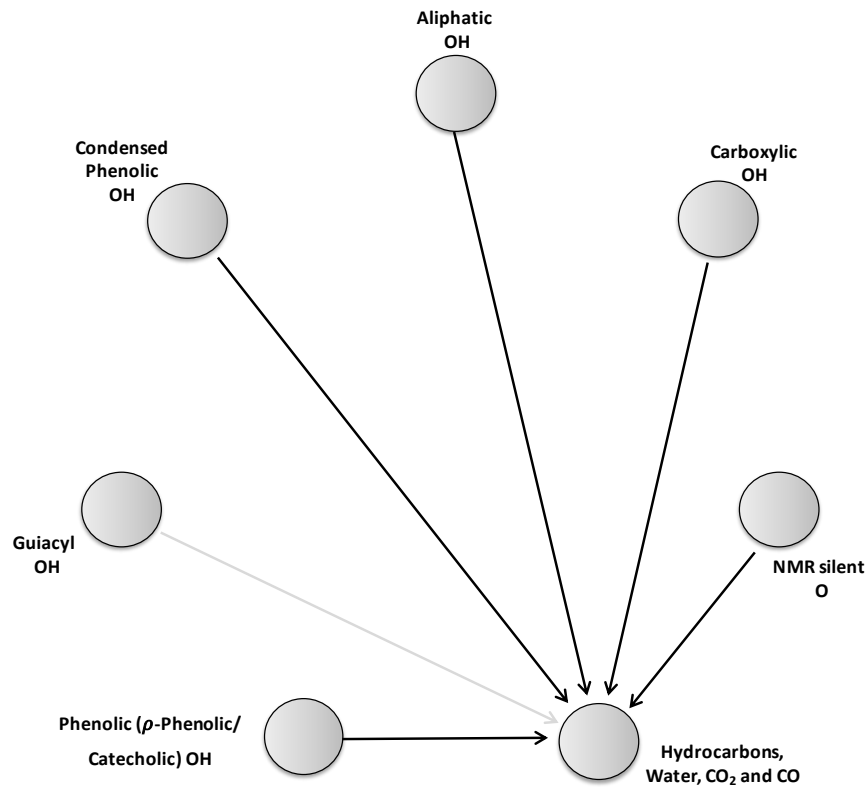
Fig. 8. The results of the parameters estimation for the network with no interconversion. The redundant arcs are shown in grey.

411   From Figure 7, it can be seen two extra reaction times at 20 and 30 minutes for Oil C are presented.

412   Despite the increased data resolution compared to Oils A and B, the computationally simulated model

413   data still failed to converge the experimentally observed concentration values for the guaiacolic and the

414   carboxylic OH groups. Moreover, the relatively large decline in Aliphatic OH concentration was not

415   associated with a large corresponding increase in the concentration of "silent" oxygens which implies

416   that they were mainly converted to hydrocarbons, water and gases.

6.2. The parameter estimation results for Network 2 with maximum connectivity

Figure 9 gives the results for the parameter estimation for Network 2, which has the maximum connectivity. However, from a study of Figure 9, it is hardly surprising that the numerically simulated data for the trial Network 2 gives the best simulation of the experimental data in Table 2. This is because Network 1 is a subset of the connectivity superstructure of Network 2.
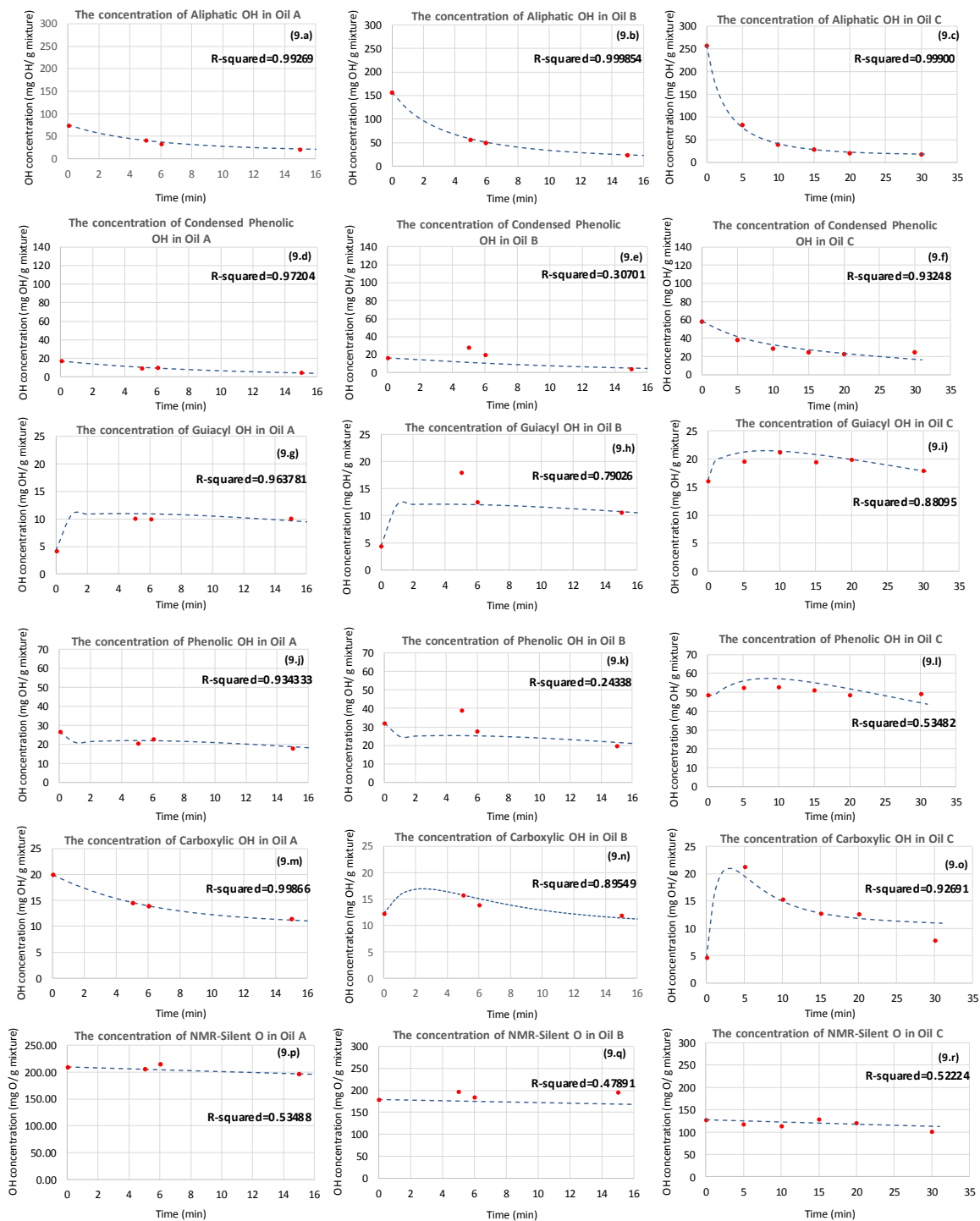
Fig. 9. The model performance for the Network 2 with maximum connectivity

424 Moreover, relative to Network 1, the simulated data for Network 2 gave an improved convergence to

425 the experimentally observed concentration changes for the Guaiacyl and Carboxylic OH group

426 elements. The best fit is for Aliphatic OH, where R-squared is larger than 0.99 in all scenarios. An

427 interesting observation is dramatic improvements in the prediction of Guiacyl OH group (R-squared:

428 0.79-0.96), which should be attributed to included interconversion pathways. Figure 10 is instructive as

429 it gives a visual representation of all kinetically redundant arcs in Network 2 which are shown in grey.

430 These were computationally calculated by using the parameter estimations based on the experimental

431 data trends in Table 2.
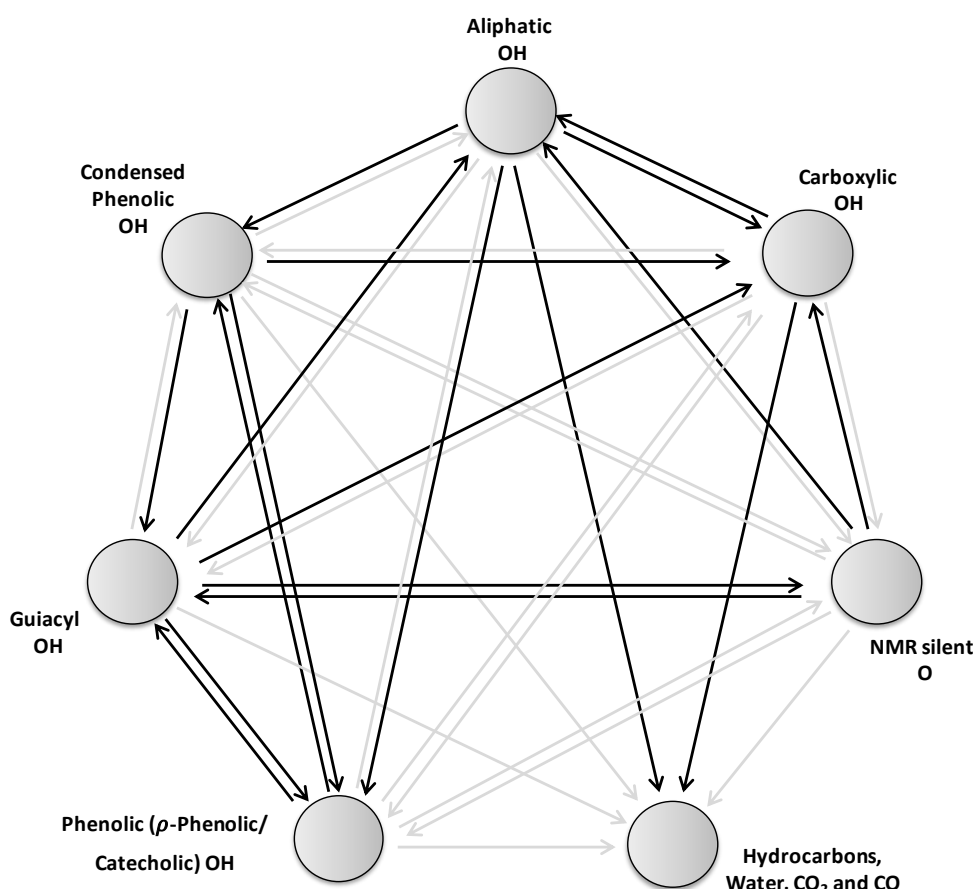
432

433 **Fig. 10** The results of the parameters estimation for Network 2 with maximum interconversion between OH
434 Group nodes. The unused arcs are shown in grey.

435 The grey arcs in Network 2 highlight the absence of reactions which lead to the conversion of (1) the

436 Aliphatic OH node to the "silent" Oxygen node, (2) the Condensed phenolic OH node to the Aliphatic

437 OH node, (3) the carboxylic OH node to "silent" oxygen node, and (4) the Guaiacyl OH node to the

438 phenolic OH node. However, the absence of these pathways are not valid as shown by their potential

439 existence by the corresponding examples in Section 5 above. An additional factor for any disparities

440 between the numerically simulated results and experimental results in Network 2 would be due to the

441   doubtful possibility of sequential reaction pathways. An example of an unlikely reaction sequence can

442   be seen by following the arrowed arcs in Figure 10, where the elements in the Condensed Phenolic OH

443   node leads to the creation of elements in a Carboxylic OHs and then to the creation of those in the

444   Aliphatic OH node. This is numerically similar to the direct conversion of elements Condensed Phenolic

445   OH node to elements reaction (R-2) in Section 5.

446   **6.3. Network 3 based on mechanistic insights: model development and parameters**

447   **estimation**

448   In view of the shortcomings of Network 2 a new trial model, Network 3, was proposed in which the

449   degrees of freedom were reduced by the omission of the least significant arcs in Network 2. Following

450   the arrows in Table 2, an attempt to link the concentration changes of elements in the Aliphatic OH

451   Group to the reversible formation of those in the Condensed Phenolic OH Group was made. A similar

452   attempt to connect irreversible oxidation of OH elements the Aliphatic OH node to those in the

453   Carboxylic OH node was also made. The development of Network 3 is based on mechanistic insights

454   gained in Section 5.
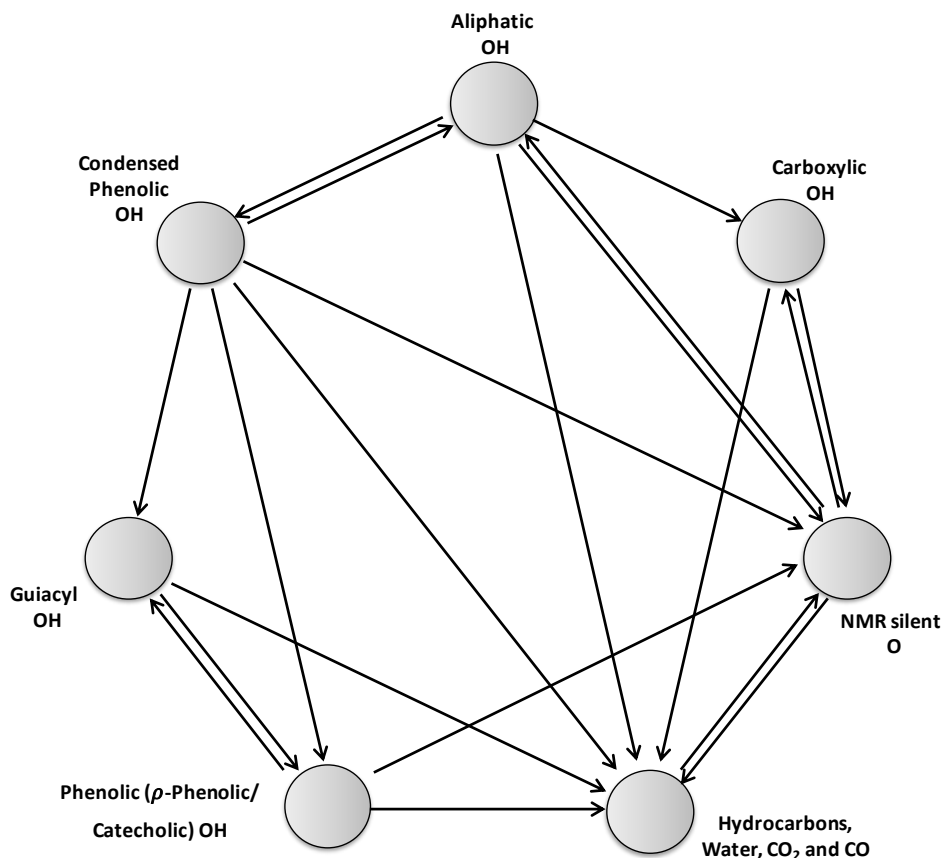
455

456   **Fig. 11** The derived trial Network 3 based on underlying chemical assumptions and the omission of the
457   computationally least significant arcs in Network 2.

458

459　Network 3 is shown in Figure 11 which also allows for the interconversion of OH groups between the

460　Aliphatic and "silent" oxygen nodes. The interconversion between the NMR "silent" node and the node

461　pertaining to water, gases and hydrocarbons was also considered.

462　According to Table 3 above, the average error of Network 3 is 4% more than Network 2 but 12% less

463　than Network 1. Figures 12 and 13 show the results of the parameter estimations for Network 3.
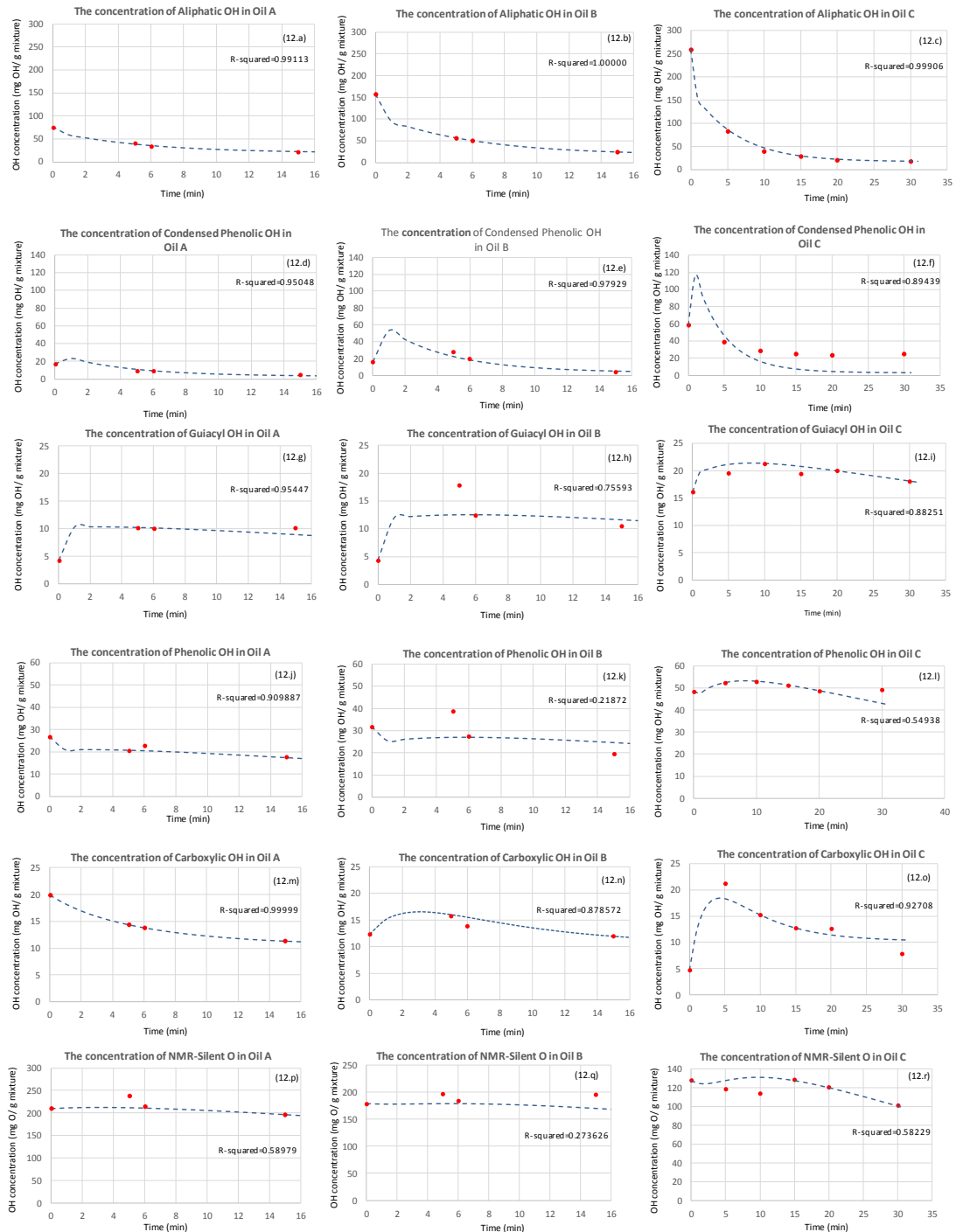
464

465　　　　　　　　**Fig. 12.** The model performance for Network 3, based on empirical insights

466 Figures 12a, b, and c suggest that the Aliphatic OH group has the highest conversion rate relative to
467 the other OH groups. The results of parameter estimations show very good fit (>0.99). The high
468 conversion of aliphatic OH is also consistent with the experimental results in Table 2. However, from a
469 consideration of the pre-exponential factors and exponents in Table S3 in the SM, it can be seen that
470 most of the aliphatic OH groups are converted to "silent" oxygens. Only a small fraction of the Aliphatic
471 OH groups converted directly to the hydrocarbons, water and gases. The implication is that Aliphatic
472 OHs are rapidly and reversibly converted to "silent" oxygens. Moreover, the interconversions of the
473 Aliphatic OH Group to the aromatic OH Group would be kinetically irrelevant. Therefore, the initial
474 increase in "silent" oxygens (Oils A and B) should be attributed to the loss of aliphatic OH groups. It is
475 notable that statistical analysis gives poor estimation for NMR-silent oxygens (R-squared: 0.27-0.59).
476 The reason should be attributed to grouping a variety of OH under this envelope. Improving the model
477 predictability would require decomposition of salient OH into sub-groups which was beyond the scope
478 of present research.

479 The oxidation of Aliphatic OH groups also gives Carboxylic OH groups as demonstrated in Section 5.2.
480 This is also shown by their initial concentration increase in Figures 12(m-o). This would account for the
481 high carboxylic OH content in oil C since the aliphatic OH content in the unprocessed oil was greater
482 than Oils A and B, also evident from Figure 3. An interesting observation was that the Genetic Algorithm
483 in MATLAB excluded the arc from Carboxylic OH Group node (grey arc in Figure 13), possibly because
484 the main acid in the upgraded Oils A, B and C was acetic acid. This is consistent with the general
485 observation that the acetic acid is stable in HCW [57].

486 Network 2 with largest connectivity (superstructure) has 108 parameters. By comparison Network 3
487 based on mechanistic insights, has only 69 parameters. In theory, and given a large amount of data the
488 two models should have converged to the same optimal structure and numerical results. However, since
489 only a limited amount of experimental data was available, the largest model was over-fitted to numerical
490 values that did not have physical significance. However, as discussed in the result section, the model
491 based on mechanistic insights has a reasonable performance.

492
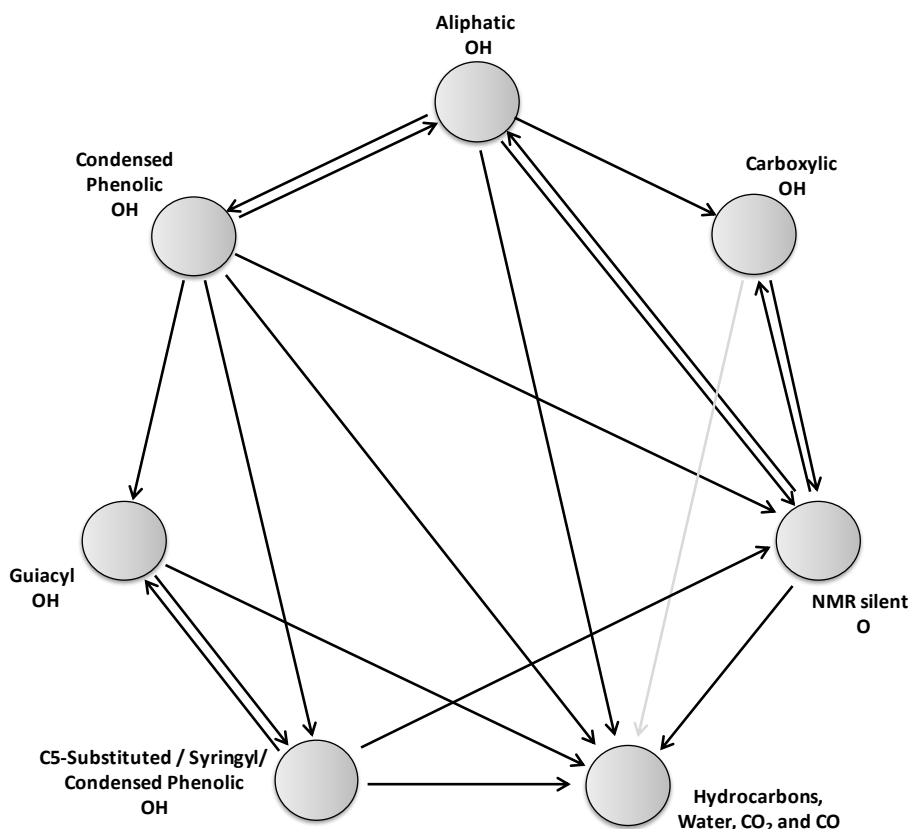
Fig. 13. The results of the parameters estimation for the Network 3 based on an empirical understanding of the underlying chemistry. The redundant arcs are shown in grey.

Amongst the various oxygenated groups in Figure 13, the "silent" organic oxygenates underwent the least conversion under the reaction conditions used. This is evident from the small pre-exponential factor of arc #6 in Table S3.

Figure 12(f) show that the simulated data did not fit the experimental data relevant to the Condensed Phenolic OH groups, possibly because they were created by the condensation of internal aliphatic OHs as for example, the reverse of reaction (R-2) in Section 5.2 above. The exact nature of the Condensed phenolic OH compounds in Oil C was beyond the scope of this work.

6. Conclusion

While, the efficiency and economic viability of hydrothermal upgrading (HTU) technology has been proposed, the experimental research needed to optimize HTU technologies often requires a time consuming and costly chemical analysis of each component in PO. Hydrothermally upgrading PO involves the chemical reactions of over 400 identified organic compounds which include esters, ethers, acids, aldehydes, ketones and alcohols [32]. Many of these chemical species are chemically unstable and undergo condensation reactions which "age" PO [58]. The diversity of PO components poses a major analytical challenge to understanding the upgrading process and hence bottleneck into the optimisation and process design of hydrothermally based upgrading technologies. To address this problem a set of preliminary "proof of concept" modelling studies were developed for the first time. The aim of this work was to investigate the potential relevance of computational modelling to highlight the significant kinetic pathways in PO deoxygenation reactions. In this paper, the overall deoxygenation kinetics of three POs called A, B and C were successfully simulated. This was achieved by using trial reaction networks and the lumped kinetic data of oils at initially known compositions. All of the necessary data needed for the computational modelling work was drawn exclusively from bespoke experiments at given reaction conditions, rather than from a literature study. The present research demonstrated that it is possible to model the main underlying kinetic pathways in deoxygenating PO by using the lumped kinetic data derived from quantitative measurements of the distribution of the organically bound OH content in intact samples of dry PO. It is anticipated that this method will afford a rapid means to screen the deoxygenation pathways of PO using only a minimum amount of experimental data. In this respect it is noteworthy the addition of two extra experimental points to Oil C did not significantly improve the performance of the computationally generated results.

OH groups are generally found in almost all of the reactive components in pyrolysis oil. Such compounds include carbohydrates which are the most reactive species under hydrothermal conditions, and also lignin-based compounds. Therefore, the characterisation of different OH groups by ^{31}P-NMR is a convenient but more importantly very efficient way to reflect the nature of pyrolysis oils [44,52] and indirectly estimate of the overall reactivity of upgrading pyrolysis oil; achieved by studying the rate at which OH groups are created or destroyed. The destruction of OH groups would occur if they produced water, gases such as CO_2 or CO, or silent species such as ethers. On the other hand, the hydrolysis of ethers (an example of NMR-silent compound) in water at around the supercritical region would produce

OH groups. The reaction of hydrocarbons with supercritical water could also produce OH groups, as for example, in the case where methane gas produces methanol [55]. Thus the water is a position donor of silent O or OH moieties to the organic makeup of upgrading oil.

Although the use of 31P NMR cannot detect silent O species, the proposed kinetic model does account for the interconversions of silent oxygen species and OH groups. This is not just a tacit assumption, as the numerical calculations involved in the formulation of the proposed reaction networks do not converge unless the silent oxygen content of the upgraded pyrolysis oils are taken into account. Unfortunately, the precise O-balance and connectivity with the oxygen routing to the gas- and solid products cannot be determined by 31P NMR, in these preliminary "proof of concept" modelling experiments, and so these parameters are simply lumped together in the underlying model structure, and deferred for future studies.

The proposed approach was deemed to be the best way to model upgrading pyrolysis oils, in which the presence of *reacting* OH groups can reflect the overall upgrading kinetics of different chemical oxygenates. Using the proposed lumped kinetic model, it was possible to treat the OH groups as a statistical population of reacting entities regardless of the precise identity of the parent molecules to which they are bonded. Therefore, the advantage of using model networks based on OH connectivity is that it was not necessary to specify exact identity of the parent molecules, which could also contain multiple OH groups, or more than one type of OH group. Each model network was only based on the connectivity of OH groups or their interconversions to "silent" oxygens. Furthermore, it was not possible to produce computationally valid solutions to the model networks without a consideration of "silent" oxygens which can also be intermediates in the non-linear and dynamic reacting populations of OH groups. Overall the deoxygenation chemistry in PO was formulated by means of a number of trial reaction networks which were used as models. Using the OH concentration changes in Table 2 for parameter estimation, (GA) was used in conjunction with the FMINCON solver to estimate the required parameters so that the differential equations relevant to the arcs in a given reaction network could be solved. The convergence of the model solutions to the experimental deoxygenation data was taken as a validation of given arcs. Starting with Networks 1 and 2, it was possible to establish the minimum degrees of freedom necessary to produce Network 3 from which it was possible to model the main kinetic pathways in Oils A, B and C, produced under different pyrolysis conditions from the same biomass.

563 Regarding Table 3, the average error of 12.96% for Network 2, in which the maximum OH connectivity

564 is considered, would be reduced by (1) the updating the ^{31}P{H} NMR protocol used and (2) increasing

565 the model resolution by, for example, quantifying the sub-groups that may be embedded in each of the

566 five OH Group classifications in Table 1. In this way the parameter estimations necessary from the

567 computation of simulated data would be enhanced. A further improvement would be to characterise the

568 ^{31}P{H} NMR-silent group using different analytical protocols. The detailed discrimination of the complex

569 interactions between ^{31}P{H} NMR-silent group and other OH groups is beyond the scope of the present

570 contribution; but is reserved for future work.

571 The ultimate aim would be devise bespoke modelling protocols from benchmark models, which could

572 then be used to predict the hydrothermally generated deoxygenation chemistry in a wider range of POs,

573 at a range of reaction conditions, regardless of the biomass used to produce them.

7. Acknowledgements

8. References

578 [1]   A. V. Bridgwater, Review of fast pyrolysis of biomass and product upgrading, Biomass and
579   Bioenergy. 38 (2012) 68–94. doi:10.1016/j.biombioe.2011.01.048.
580 [2]   S. Czernik, a V Bridgwater, Overview of applications of biomass fast pyrolysis oil, Energy &
581   Fuels. 18 (2004) 590–598. doi:Doi 10.1021/Ef034067u.
582 [3]   G.W. Huber, S. Iborra, A. Corma, Synthesis of Transportation Fuels from Biomass: Chemistry,
583   Catalysts, and Engineering, Chem. Rev. 106 (2006) 4044–4098. doi:10.1021/cr068360d.
584 [4]   D. Mohan, C.U.J. Pittman, P.H. Steele, Pyrolysis of Wood/Biomass for Bio-oil: A Critical
585   Review, Energy & Fuels. 20 (2006) 848–889. doi:10.1021/ef0502397.
586 [5]   M. Sharifzadeh, C.J. Richard, K. Liu, K. Hellgardt, D. Chadwick, N. Shah, An integrated
587   process for biomass pyrolysis oil upgrading: A synergistic approach, Biomass and Bioenergy.
588   76 (2015) 108–117.
589 [6]   M. Sharifzadeh, L. Wang, N. Shah, Integrated biorefineries: CO_2 utilization for
590   maximum biomass conversion, Renew. Sustain. Energy Rev. 47 (2015).
591   doi:10.1016/j.rser.2015.03.001.
592 [7]   M. Sharifzadeh, L. Wang, N. Shah, Decarbonisation of olefin processes using biomass
593   pyrolysis oil, Appl. Energy. 149 (2015) 404–414.
594 [8]   M. Sharifzadeh, M.C. Garcia, N. Shah, Supply chain network design and operation: Systematic
595   decision-making for centralized, distributed, and mobile biofuel production using mixed integer

596   linear programming (MILP) under uncertainty, Biomass and Bioenergy. 81 (2015).

597   doi:10.1016/j.biombioe.2015.07.026.

598   [9]   J.D. Rocha, C.A. Luengo, C.E. Snape, The scope for generating bio-oils with relatively low

599   oxygen contents via hydropyrolysis, Org. Geochem. 30 (1999) 1527–1534.

600   doi:10.1016/S0146-6380(99)00124-2.

601   [10]   Q. Zhang, J. Chang, T. Wang, Y. Xu, Review of biomass pyrolysis oil properties and upgrading

602   research, Energy Convers. Manag. 48 (2007) 87–92. doi:10.1016/j.enconman.2006.05.010.

603   [11]   P. Grange, E. Laurent, R. Maggi, A. Centeno, B. Delmon, Hydrotreatment of pyrolysis oils from

604   biomass: reactivity of the various categories of oxygenated compounds and preliminary

605   techno-economical study, Catal. Today. 29 (1996) 297–301. doi:10.1016/0920-

606   5861(95)00295-2.

607   [12]   T.P. Vispute, H. Zhang, A. Sanna, R. Xiao, G.W. Huber, Renewable chemical commodity

608   feedstocks from integrated catalytic processing of pyrolysis oils, Science. 330 (2010) 1222–

609   1227. doi:10.1126/science.1194218.

610   [13]   E. Laurent, B. Delmon, Influence of water in the deactivation of a sulfided NiMoγ-Al2O3

611   catalyst during hydrodeoxygenation, J. Catal. 146 (1994) 281–291. doi:10.1016/0021-

612   9517(94)90032-9.

613   [14]   D.C. Elliott, Historical Developments in Hydroprocessing Bio-oils, Energy & Fuels. 21 (2007)

614   1792–1815. doi:10.1021/ef070044u.

615   [15]   E. BERL, Production of oil from plant material, Science (80-.). 99 (1944) 309–312.

616   doi:10.1126/science.99.2573.309.

617   [16]   F. Goudnaan, B. van de Beld, F.R. Boerefijn, G.M. Bos, J.E. Naber, S. van der Wal, J.A.

618   Zeevalkink, Thermal Efficiency of the HTU® Process for Biomass Liquefaction, in: A. V.

619   Bridgwater (Ed.), Prog. Thermochem. Biomass Convers., Wiley Blackwell, 2008: pp. 1312–

620   1325.

621   [17]   E. Ulrich Franck, Fluids at high pressures and temperatures, J. Chem. Thermodyn. 19 (1987)

622   225–242. doi:10.1016/0021-9614(87)90130-3.

623   [18]   C.J. Richard, B. Patel, D. Chadwick, K. Hellgardt, Hydrothermal deoxygenation of pyrolysis oil

624   from Norwegian spruce: Picea abies, Biomass and Bioenergy. 56 (2013) 446–455.

625   [19]   J.E. White, W.J. Catallo, B.L. Legendre, Biomass pyrolysis kinetics: A comparative critical

626   review with relevant agricultural residue case studies, J. Anal. Appl. Pyrolysis. 91 (2011) 1–33.

627   doi:10.1016/j.jaap.2011.01.004.

628   [20]   F. Shafizadeh, Introduction to pyrolysis of biomass, J. Anal. Appl. Pyrolysis. 3 (1982) 283–305.

629   doi:10.1016/0165-2370(82)80017-X.

630   [21]   H. Yang, R. Yan, H. Chen, C. Zheng, Dong Ho Lee, and David Tee Liang, In-Depth

631   Investigation of Biomass Pyrolysis Based on Three Major Components: Hemicellulose,

632   Cellulose and Lignin, Energy & Fuels. 20 (2006) 388–393. doi:10.1021/ef0580117.

633   [22]   X. Besse, Y. Schuurman, N. Guilhaume, Hydrothermal conversion of linoleic acid and ethanol

634   for biofuel production, Appl. Catal. A Gen. 524 (2016) 139–148.

635   [23]   A.A. Peterson, R.P. Lachance, J.W. Tester, Kinetic Evidence of the Maillard Reaction in

636   Hydrothermal Biomass Processing: Glucose−Glycine Interactions in High-Temperature, High-

637   Pressure Water, Ind. Eng. Chem. Res. 49 (2010) 2107–2117. doi:10.1021/ie9014809.

638   [24]   N. Abatzoglou, E. Chornet, K. Belkacemi, R.P. Overend, Phenomenological kinetics of

639   complex systems: the development of a generalized severity parameter and its application to

640   lignocellulosics fractionation, Chem. Eng. Sci. 47 (1992) 1109–1122.

641   [25]   R.P. Overend, E. Chornet, J.A. Gascoigne, Fractionation of Lignocellulosics by Steam-

642   Aqueous Pretreatments [and Discussion], Philos. Trans. R. Soc. London A Math. Phys. Eng.

643   Sci. 321 (1987) 523–536. doi:10.1098/rsta.1987.0029.

644   [26]   J. Zhang, B. Jiang, D. Wang, Thermogravimetric and kinetic analysis of bio-crude from

645   hydrothermal liquefaction of Enteromorpha prolifera, Algal Res. 18 (2016) 45–50.

646   [27]   T.K. Vo, O.K. Lee, E.Y. Lee, C.H. Kim, J.-W. Seo, J. Kim, S.-S. Kim, Kinetics study of the

647   hydrothermal liquefaction of the microalga Aurantiochytrium sp. {KRS101}, Chem. Eng. J. 306

648   (2016) 763–771. doi:http://dx.doi.org/10.1016/j.cej.2016.07.104.

649   [28]   D.C. Hietala, J.L. Faeth, P.E. Savage, A quantitative kinetic model for the fast and isothermal

650   hydrothermal liquefaction of Nannochloropsis sp., Bioresour. Technol. 214 (2016) 102–111.

651   [29]   P.J. Valdez, V.J. Tocco, P.E. Savage, A general kinetic model for the hydrothermal

652   liquefaction of microalgae, Bioresour. Technol. 163 (2014) 123–127.

653   [30]   L. Luo, L. Dai, P.E. Savage, Catalytic hydrothermal liquefaction of soy protein concentrate,

654   Energy and Fuels. 29 (2015) 3208–3214.

655   [31]   F. Yin, H. Chen, G. Xu, G. Wang, Y. Xu, A detailed kinetic model for the hydrothermal

656   decomposition process of sewage sludge, Bioresour. Technol. 198 (2015) 351–357.

657   [32]   T. Milne, F. Agblevor, M. Davis, S. Deutch, D. Johnson, A Review of the Chemical

658   Composition of Fast-Pyrolysis Oils from Biomass, in: A. V Bridgwater, D.G.B. Boocock (Eds.),

659   Dev. Thermochem. Biomass Convers., Springer Netherlands, Dordrecht, 1997: pp. 409–424.

660   doi:10.1007/978-94-009-1559-6_32.

661   [33]   Qirong Fu, D.S. Argyropoulos, David C. Tilotta, Lucian A. Lucia, Products and Functional

662   Group Distributions in Pyrolysis Oil of Chromated Copper Arsenate (CCA)-Treated Wood, as

663   Elucidated by Gas Chromatography and a Novel 31P NMR-Based Method, Ind. Eng. Chem.

664   Res. 46 (2007) 5258–5264. doi:10.1021/ie0702274.

665   [34]   C. Lensink, J.G. Verkade, Phosphorus-31 NMR spectroscopic analysis of labile hydrogen

666   functional groups: identification with a dithiaphospholane reagent, Energy & Fuels. 4 (1990)

667   197–201. doi:10.1021/ef00020a012.

668   [35]   A.E. Wroblewski, C. Lensink, R. Markuszewski, J.G. Verkade, Phosphorus-31 NMR

669   spectroscopic analysis of coal pyrolysis condensates and extracts for heteroatom

670   functionalities possessing labile hydrogen, Energy & Fuels. 2 (1988) 765–774.

671   doi:10.1021/ef00012a008.

672   [36]   K. Erdmann, T. Mohan, J.G. Verkade, HPLC and 31P NMR Analysis of Phenols in Coal

673   Liquefaction Oils, Energy & Fuels. 10 (1996) 378–385. doi:10.1021/ef950122q.

674   [37]   H. Ben, A.J. Ragauskas, NMR Characterization of Pyrolysis Oils from Kraft Lignin, Energy &

675   Fuels. 25 (2011) 2322–2332. doi:10.1021/ef2001162.

676 [38] M. Nagy, B.J. Kerr, C.J. Ziemer, A.J. Ragauskas, Phosphitylation and quantitative 31P {NMR}
677   analysis of partially substituted biodiesel glycerols, Fuel. 88 (2009) 1793–1797.
678   doi:10.1016/j.fuel.2009.01.020.
679 [39] C. Crestini, D.S. Argyropoulos, Structural Analysis of Wheat Straw Lignin by Quantitative 31P
680   and 2D NMR Spectroscopy. The Occurrence of Ester Bonds and α-O-4 Substructures, J.
681   Agric. Food Chem. 45 (1997) 1212–1219. doi:10.1021/jf960568k.
682 [40] D.S. Argyropoulos, Quantitative Phosphorus-31 NMR Analysis of Lignins, a New Tool for the
683   Lignin Chemist, J. Wood Chem. Technol. 14 (1994) 45–63. doi:10.1080/02773819408003085.
684 [41] D.C. Elliott, Catalytic hydrothermal gasification of biomass, Biofuels, Bioprod. Biorefining. 2
685   (2008) 254–265. doi:10.1002/bbb.74.
686 [42] R. Ibbett, S. Gaddipati, S. Davies, S. Hill, G. Tucker, The mechanisms of hydrothermal
687   deconstruction of lignocellulose: New insights from thermal–analytical and complementary
688   studies, Bioresour. Technol. 102 (2011) 9272–9278.
689   doi:http://dx.doi.org/10.1016/j.biortech.2011.06.044.
690 [43] K. Freudenberg, A.C. Neish, Constitution and Biosynthesis of Lignin, Springer-Verlag, New
691   York, 1968.
692 [44] K. David, M. Kosa, A. Williams, R. Mayor, M. Realff, J. Muzzy, A. Ragauskas, 31P-NMR
693   analysis of bio-oils obtained from the pyrolysis of biomass, Biofuels. 1 (2010) 839–845.
694   doi:10.4155/bfs.10.57.
695 [45] A.R. Katritzky, M. Balasubramanian, M. Siskin, Aqueous high-temperature chemistry of carbo-
696   and heterocycles. 2. Monosubstituted benzenes: benzyl alcohol, benzaldehyde and benzoic
697   acid, Energy & Fuels. 4 (1990) 499–505. doi:10.1021/ef00023a016.
698 [46] M. Siskin, G. Brons, A.R. Katritzky, M. Balasubramanian, Aqueous organic chemistry. 1.
699   Aquathermolysis: comparison with thermolysis in the reactivity of aliphatic compounds, Energy
700   & Fuels. 4 (1990) 475–482. doi:10.1021/ef00023a012.
701 [47] M.A. DeSilva, N. Shanaiah, G.A. Nagana Gowda, K. Rosa-Pérez, B.A. Hanson, D. Raftery,
702   Application of 31P NMR spectroscopy and chemical derivatization for metabolite profiling of
703   lipophilic compounds in human serum, Magn. Reson. Chem. 47 (2009) S74--S80.
704   doi:10.1002/mrc.2480.
705 [48] K. Arai, T. Adschiri, Masaru Watanabe, Hydrogenation of Hydrocarbons through Partial
706   Oxidation in Supercritical Water, Ind. Eng. Chem. Res. 39 (2000) 4697–4701.
707   doi:10.1021/ie000326g.
708 [49] S.A. Hosseini, R. Lambert, S. Kucherenko, N. Shah, Multiscale Modeling of Hydrothermal
709   Pretreatment: From Hemicellulose Hydrolysis to Biomass Size Optimization, Energy & Fuels.
710   24 (2010) 4673–4680. doi:10.1021/ef9012246.
711 [50] H.A. Ruiz, R.M. Rodríguez-Jasso, B.D. Fernandes, A.A. Vicente, J.A. Teixeira, Hydrothermal
712   processing, as an alternative for upgrading agriculture residues and marine biomass according
713   to the biorefinery concept: A review, Renew. Sustain. Energy Rev. 21 (2013) 35–51.
714   doi:http://dx.doi.org/10.1016/j.rser.2012.11.069.
715 [51] S.H. Townsend, M.A. Abraham, G.L. Huppert, M.T. Klein, S.C. Paspek, Solvent effects during

716   reactions in supercritical water, Ind. Eng. Chem. Res. 27 (1988) 143–149.

717   doi:10.1021/ie00073a026.

718   [52] K. David, H. Ben, J. Muzzy, C. Feik, K. Iisa, A. Ragauskas, Chemical characterization and

719   water content determination of bio-oils obtained from various biomass species using 31P NMR

720   spectroscopy, Biofuels. 3 (2012). doi:10.4155/BFS.12.1.

721   [53] M. Siskin, A.R. Katritzky, M. Balasubramanian, Aqueous organic chemistry. 4. Cleavage of

722   diaryl ethers, Energy & Fuels. 5 (1991) 770–771. doi:10.1021/ef00029a028.

723   [54] A.H. Wright, Genetic algorithms for real parameter optimization, Found. Genet. Agorithms. 1

724   (1990) 205–220. doi:citeulike-article-id:1439583.

725   [55] P.E. Savage, R. Li, J.T. Santini, Methane to methanol in supercritical water, J. Supercrit.

726   Fluids. 7 (1994) 135–144.

727   [56] K.S. Shin, H.Y. Cho, Y.W. Nam, D.S. Lee, Hydrothermal Decomposition of Formic Acid in Sub-

728   and Supercritical Water, Environ. Eng. Res. 3 (1998) 61–66. doi:10.1021/ef9005093.

729   [57] M. Watanabe, H. Inomata, R.L. Smith, K. Arai, Catalytic decarboxylation of acetic acid with

730   zirconia catalyst in supercritical water, Appl. Catal. A Gen. 219 (2001) 149–156.

731   doi:10.1016/S0926-860X(01)00677-9.

732   [58] C.A. Fisk, T. Morgan, Y. Ji, M. Crocker, C. Crofcheck, S.A. Lewis, Bio-oil upgrading over

733   platinum catalysts using in situ generated hydrogen, Appl. Catal. A Gen. 358 (2009) 150–156.

734